Tanguy Mertens

A new mapped infinite partition of unity method for convected acoustical radiation in infinite domains.

January 20, 2009

Université Libre de Bruxelles

Remerciements

Si tu donnes un poisson à un homme, il ne mangera qu'un jour. S'il apprend à pêcher, il mangera toute sa vie.

Proverbe de Confucius, repris plus tard par Dominique Pire dans le cadre de l'action Iles de Paix.

Je remercie Philippe Bouillard de m'avoir donné ma canne à pêche et conduit à l'étang. Je remercie Laurent Hazard et Guy Paulus pour tous leurs conseils avisés. Et tous les autres, famille, amis, qui ont gardé confiance en moi et m'ont encouragé à la persévérance.

C'est grâce à vous tous que je peux vous présenter avec fierté mon premier poisson.

Ceci dit, je voudrais remercier de manière plus académique tous les acteurs du projet.

Je remercie Philippe Bouillard qui est à la source du projet et qui a contribué à mon épanouissement scientifique durant cette aventure au sein du service BATir. Je remercie également pour leur encadrement: Guy Warzée pour sa gentillesse et sa patience ainsi que Jean-Louis Migeot pour son soutien industriel et ses remarques pertinentes.

Ce passage au service BATir a été une expérience riche sur le plan scientifique mais aussi humain. Je remercie mes collègues de l'ULB pour les relations que nous avons construites ensemble, pour les activités dans le cadre du travail ou hors des murs de l'université. Je pense évidemment à Laurent Hazard et à Guy Paulus, pour leur amitié mais aussi leur disponibilité et leurs nombreux conseils. Merci aussi à tous les membres du service des milieux continus qui ont ajouté une dimension humaine. La nature des contrats de recherche et d'assistanat est tel qu'ils furent nombreux a être passés par les murs de l'université. Je ne pourrai tous les citer mais je tiens quand même à remercier personellement Katy, Erik, Geneviève, Yannick, Louise, Dominique, Thierry, Sandrine, Bertha, David, Benoît, Peter et Kfir.

S'il est vrai qu'un travail de thèse tend à rendre le chercheur autonome, les collaborations et interactions restent importantes. Je remercie à cet égard toute l'équipe de l'Institute of Sound and Vibration Research de l'université de Southampton. Je remercie Jeremy Astley, chef du service de m'y avoir accueilli pendant un stage de six mois. Je le

remercie aussi pour l'environnement de travail de qualité qu'il m'a offert. Il est évident que la présence de Pablo Gamallo à l'I.S.V.R. a énormément contribué à l'aboutissement de ce travail de recherche. Je le remercie pour tout le temps qu'il m'a consacré, à Southampton et même par la suite lors de contacts e-mail ou lors de rencontres en conférences. Je le remercie pour l'intérêt qu'il porte à la présente étude, pour ses encouragements et pour tous ses enseignements. Mais ce séjour n'a pas été que professionellement enrichissant, je repense à l'accueil qui m'a été réservé ainsi que de nombreux excellents souvenirs qui font de ce séjour une partie inoubliable de ma vie. Je tiens donc à remercier chaleureusement pour leur amitié précieuse Vincent et Theresa, Luigi, Claire, Naoki, Rie, Sue, Lisa, Eugene, Isa, Daniel et Stéphanie, Alessandro et Emmet.

Ces quelques lignes indiquent à quel point les relations humaines ont une influence sur ma vie. Cela ne sera pas une surprise alors si je remercie les personnes pour qui je *travaille dans les avions* ou ceux qui me félicitent de mon travail, *les semaines durant lesquelles, ils n'ont pas trop entendu les avions*. Je pense bien entendu à ma famille, principalement ma maman, pour avoir fait de moi l'homme que je suis aujourd'hui et mes amis, plus particulièrement mes collocataires: Iyad, Mathieu, Quentin, Guerrick, Caroline et Florence. Merci à vous de partager mes valeurs et de colorier mon existence.

Enfin, je terminerai par remercier les deux petits rayons de soleil qui ont ensoleillé la fin de ce long parcours.

List of Symbols

Greek symbols

β	: $\sqrt{1-M_0^2}$	
γ	: Poisson ratio of specific heat capacities : c_p/c_v	
Γ	: interface separating the inner and the outer domains	
ε	: Error	
μ	: phase function	$[m]$
ρ	: mass density	$[kgm^{-3}]$
ρ_0	: steady mean density	$[kgm^{-3}]$
ρ_a	: acoustic density	$[kgm^{-3}]$
$\boldsymbol{\sigma}$	: stress tensor	$[Nm^{-2}]$
ϕ	: velocity potential	$[m^2s^{-1}]$
ϕ_0	: mean velocity potential	$[m^2s^{-1}]$
ϕ_a	: acoustic velocity potential	$[m^2s^{-1}]$
$\tilde{\phi}_a$	: amplitude of the harmonic acoustic velocity potential	$[m^2s^{-1}]$
$\tilde{\phi}^h$	: numerical approximation of $\tilde{\phi}_a$	$[m^2s^{-1}]$
$\tilde{\phi}_h^I$	: numerical approximation in the outer region Ω_o	$[m^2s^{-1}]$
Φ_α	: shape function for the α^{th} degree of freedom	
Φ_α^I	: infinite shape function for the α^{th} degree of freedom	
ω	: angular frequency	$[s^{-1}]$
Ω	: domain	
Ω_i	: inner region	
Ω_o	: outer region	

Arabic symbols

$\tilde{a}_n$	: normal acceleration of a vibrating wall	$[ms^{-2}]$
A_n	: normal acoustic admittance	$[m^2skg^{-1}]$
$A^{\pm}_{mn}$	: incident and reflected modal amplitude	$[m^2s^{-1}]$
c	: speed of sound	$[ms^{-1}]$
c_0	: steady mean part of the speed of sound	$[ms^{-1}]$
c_∞	: speed of sound at large distance from the source	$[ms^{-1}]$
c_p	: specific heat capacity at constant pressure	$[JK^{-1}]$
c_v	: specific heat capacity at constant volume	$[JK^{-1}]$
$dofs$	: number of unknowns of the approximation	
E	: energy flow out of a surface	$[J]$
$E^{\pm}_{mn}$	: incident and reflected modal patern	
f	: excitation frequency	$[s^{-1}]$
G	: geometric factor	
h	: mesh size	$[m]$
H	: Hilbert space	
i	: imaginary unit $= \sqrt{-1}$	
$\mathbf{I}$	: Sound intensity	$[Wm^{-2}]$
J'	: stagnation entropy	$[Jkg^{-1}]$
k	: wavenumber	$[m^{-1}]$
$k^{\pm}_{r,mn}$	: incident and reflected radial wavenumber	$[m^{-1}]$
k_B	: Boltzmann constant	$[JK^{-1}]$
$K^{\pm}_{z,mn}$	: incident and reflected axial wavenumber	$[m^{-1}]$
L^d_j	: Legendre polynomial of order d for node j	
L_s	: curve enclosing the boundary S_s	
L_v	: curve enclosing the boundary S_v	
m	: angular mode number	
$\mathbf{m}'$	: mass flux	$[kgm^-2s^{-1}]$
m_0	: radial order of the infinite element	
m_w	: mass of a molecule	$[kg]$
M_0	: mach number	
M_i	: Mapping function for node/point i	
$\mathbf{n}$	: outer normal to the domain	
n	: radial mode number	
n^I_d	: number of infinite degree of freedom	
$n(j)$	: size of the local approximation space at node j	
nni	: number of infinite nodes	
$nodes$	: number of nodes	
N_i	: Partition of Unity function of node i	
N_m	: number of angular modes	
N_n	: number of radial modes	
N_M	: number of reflected modes (unknown)	

p	: fluid pressure	$[Pa]$
p_0	: steady mean fluid pressure	$[Pa]$
p_a	: acoustic pressure	$[Pa]$
$\tilde{p}_a$	: amplitude of the harmonic acoustic pressure	$[Pa]$
$\tilde{p}_{an}$	: analytic amplitude of the harmonic acoustic pressure	$[Pa]$
$\mathbf{q}$	: heat flux	$[Wm^{-2}]$
Q_w	: heat production	$[J]$
r_o	: distance to the source point	$[m]$
R	: specific gas constant	$[JK^{-1}mol^{-1}]$
R_j	: radial function for infinite node j	
R_j^d	: radial function of order d for node j	
s	: entropy	$[Jkg^{-1}K^{-1}]$
S	: boundary	
S_i	: mapping functions for the interface $\mathit{\Gamma}$	
S_M	: Modal boundary	
S_s	: soft wall	
S_v	: vibrating wall	
t	: time	$[s]$
T	: Temperature	$[K]$
T_j	: circumferential function for infinite node j	
$\tilde{u}_n$	: normal displacement of a vibrating wall	$[m]$
$\mathbf{v}$	: fluid velocity	$[ms^{-1}]$
$\mathbf{v}_0$	: steady mean fluid velocity	$[ms^{-1}]$
$\mathbf{v}_\infty$	: fluid velocity at large distance from the source	$[ms^{-1}]$
$\mathbf{v}_a$	: acoustic velocity	$[ms^{-1}]$
$\tilde{\mathbf{v}}_a$	: amplitude of the harmonic acoustic velocity	$[ms^{-1}]$
$\mathscr{V}$	: the Sobolev space $W^{1,2} = H^1 = \{f : f, \nabla f \in L^2\}$	
V_{jl}	: l^{th} local approximation function of node j	
$\tilde{w}_n$	: normal velocity of a vibrating wall	$[ms^{-1}]$
W_j	: weight function of node j	
W_j^I	: infinite weight function of the infinite node j	
$W_{M,nm}$	: modal weight function of the angular and radial mode (m,n)	

Operators

∇	: gradient operator
$\nabla\cdot$	: divergence operator
$\nabla\times$	: curl operator
$\mathit{\Delta}$	: Laplacian operator
$\frac{D}{Dt}$	: Total time derivative
$:$	: the double dot product of two tensors
$\langle\ \rangle$	: time average
$\Re$	: Real part

Contents

6

Three-dimensional formulation: performance analysis

This chapter analyses the performances of the Mapped Infinite Partition of Unity Method for three-dimensional applications. We deal with inner and exteriors applications and compare the accuracy and the efficiency of the method for different enrichments.

The characteristics of the computer are given in chapter 5. The analytical solutions of the applications analysed in this chapter are detailed in sections 5.1 for duct propagation and 3.3 for multipole radiation.

6.1 Duct propagation

In this section, we investigate the performances of the Mapped Infinite Partition of Unity Method in inner regions. We consider acoustic propagation in straight ducts of infinite length. Analyses are performed on ducts with circular, rectangular and annular cross-sections. Note that we compute ducts of finite length with boundary conditions simulating infinite propagation. This is done in this section by prescribing either modal or Neumann boundary conditions.

6.1.1 Circular cross-section

A convergence analysis is performed to evaluate the efficiency of some enrichments. We consider the propagation at 800 Hz of the second radial mode ($n = 2$) of the first azimuthal order ($m = 1$). This is prescribed with modal and transmitted boundary conditions. Figure 6.1 illustrates the L^2 relative error with respect to the number of degrees of freedom. The number of elements in the axial direction is taken proportional to $3j$ and those in the cross-section $j \times j$ (j being a parameter of the convergence analysis). Note that we do not generate these meshes for the cubic enrichment. In this last case, we use $2j + 2$ elements along the axial direction and $j + 2 \ \times \ j + 2$ elements in the cross-section. The cubic enrichment requires less elements to be accurate (lower j). The aim is then to ensure a good representation of the section, even for low number of elements in the axial direction.

Figure 6.1 illustrates the same behaviour as those we observed for axisymmetric applications: the highest order for the enrichment leads to the most accurate solution and the best convergence rate.

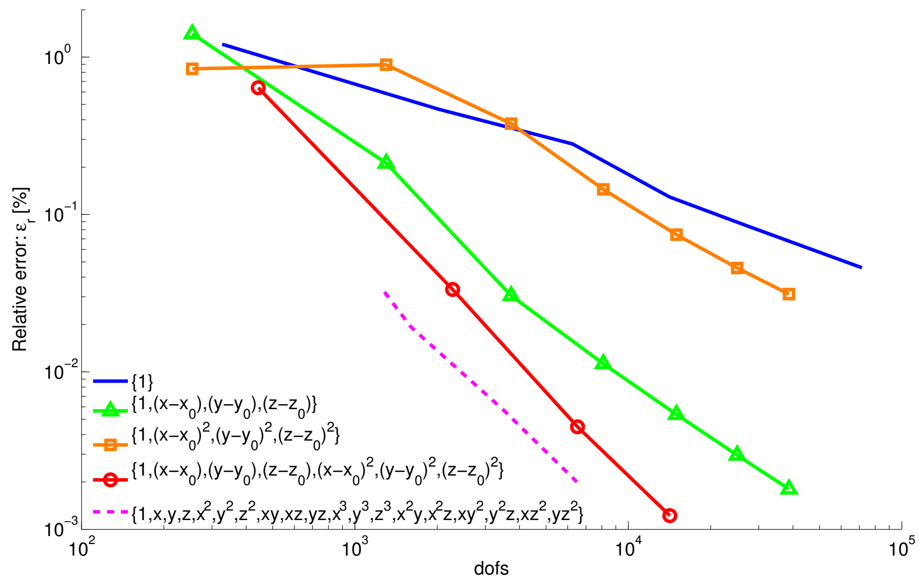

Fig. 6.1. Relative error ($\varepsilon_r = 1$ *means* 100% of error) plotted with respect to the number of degrees of freedom (dofs): propagation of the second mode ($n = 2$), first axisymetric order ($m = 1$) and excitation frequency 800 Hz ($kR_d = 7.39$) (Some simplifications have been made in the legend. The terms $\{x, y, ...\}$ of the cubic enrichment have to be read as $\{(x - x_0), (y - y_0), ...\}$)

A performance analysis (figure 6.2) is performed to compare the efficiency of the method in terms of computational time. This is the reason why we plot the computational time with respect to the non-dimensional wavenumber (kD). The computational time corresponds to the time required to generate the mesh, compute the matrices of the system and solve the application with a given kD such that the accuracy (L^2 relative error) remains bounded: $\varepsilon_r \leq 5\%$. The mesh is chosen to have $2j$ elements along the axial direction and $j \times j$ within the cross-section. We observe, as it is illustrated for axisymmetric models, that it is more convenient to use high order enrichments. For the same amount of CPU time, higher frequencies can be computed with higher enrichment order. It is expected that higher order requires less computational time for the same accuracy. In figure 6.2, we try to compare different solutions with the same level of accuracy. However, it is not the case for third order polynomial enrichments[1], which explains why it is more time consuming. We may also conclude that the computation for a given excitation frequency requires less computational time for higher enrichment orders. The required CPU time increases exponentially with respect to the non-dimensional wavenumber kD. It is obvious that computations would

[1] In the case of $p = 3$, the accuracy is close to 1% while it is close to 5% for the second order enrichment.

require huge amount of time as soon as we exceed $kD = 10$ for the constant enrichment (degenerated linear FEM). In the case of higher order enrichments, this limit is moved to higher non-dimensional wavenumbers (kD 45).

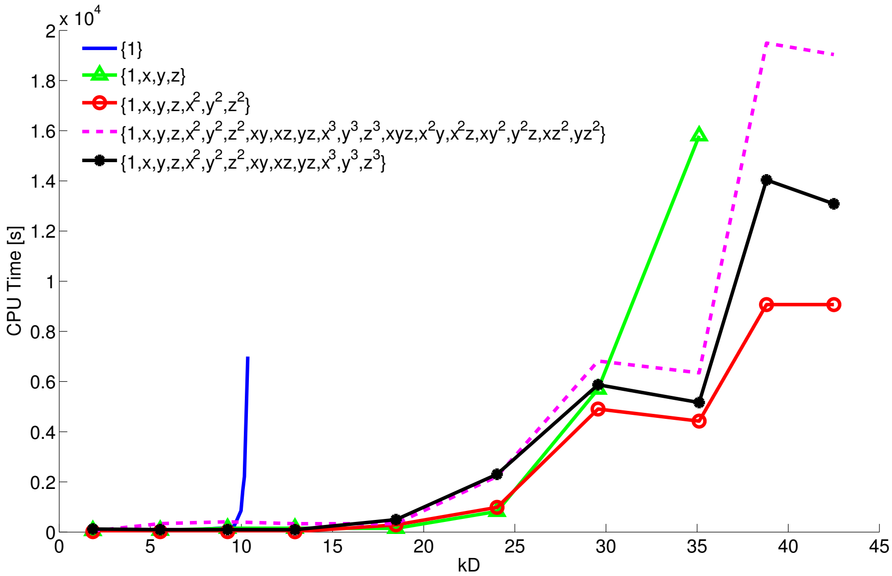

Fig. 6.2. Evolution of the computational Time (s) versus the non-dimensional wavenumber (kD) with an accuracy under 5%, frequency varying from 100Hz to 2300Hz ($560Hz$ *for the constant enrichment:* $V_{jl} = \{1\}$), the characteristic length $D = 1m$ is the diameter of the duct.(Some simplifications have been made, terms of the legend such as $\{x, y, ...\}$ have to be read as $\{(x - x_0), (y - y_0), ...\}$)

Tables 6.1, 6.2 and 6.3 give results coming from the previous performance analysis. Each table presents results obtained for different enrichments: constant, second order and third order enrichments. The tables give, for several frequencies, the required number of elements and degrees of freedom required to solve the application within an accuracy of less than 5%. The tables also illustrate the level of relative error reached[2] with this mesh and the CPU time required.

For the constant enrichment (table 6.1), we observe that the number of degrees of freedom required to ensure an accuracy below 5% increases a lot compared to those required for higher order enrichments: at $500Hz$, 23807 degrees of freedom are required for the constant enrichment while only 786 and 2242 degrees of freedom are required for the second and third order enrichments, respectively. This corresponds to more than a factor 10!

We show that for the same number of degrees of freedom, the computational error is lower for high order enrichments (figure 6.1). But we also observe that for the same

[2] An iterative approach on the mesh parameter j to find, at each frequency, the mesh giving an accuracy below 5% but as close as possible to this value. For high order enrichment functions, an admissible mesh parameter j could lead to a relative error smaller than the prescribed 5% see table 6.3

number of degrees of freedom, the CPU time required to compute a solution increases with the order of the enrichment. The constant enrichment requires 18s to compute the solution for a system of 5294 degrees of freedom. The second order enrichment requires 987s for a system of 4461 degrees of freedom and 2218s for 4502 degrees of freedom in the case of a third order enrichment. However, we finally illustrated that for the same level of accuracy, it is more convenient to compute the solution with a high order enrichment (figure 6.2). This can be explained by comparing the huge number of degrees of freedom required for the constant enrichment with higher order ones.

Frequency (Hz)	Elements	Dofs	CPU time (s)	ε_r (%)
100	2662	3314	9	4.29
300	4394	5294	18	4.54
500	21296	23807	170	5
520	27648	30627	252	4.83
540	54000	58623	852	4.78
545	65536	70787	1653	4.93
550	93312	99939	2210	4.72
560	170368	180227	6996	4.84

Table 6.1. Results of the performance analysis of the cylindrical duct with a circular cross-section for the constant enrichment $\{1\}$

Frequency (Hz)	Elements	Dofs	CPU time (s)	ε_r (%)
100	54	786	19	2.98
300	54	786	16	2.62
500	54	786	16	1.77
700	54	786	15	4.77
1000	250	2774	286	4.88
1300	432	4461	987	4.75
1600	1024	9641	4905	3.98
1900	1024	9641	4423	4.52
2100	1458	13302	9067	3.29
2300	1458	13302	9069	4.89

Table 6.2. Results of the performance analysis of the circular duct for the second order enrichment $\left\{1, (x-x_0), (y-y_0), (z-z_0), (x-x_0)^2, (y-y_0)^2, (z-z_0)^2\right\}$

Frequency (Hz)	Elements	Dofs	CPU time (s)	ε_r (%)
100	16	902	46	4.67
300	54	2242	337	1
500	54	2242	412	1.96
700	54	2242	332	1.42
1000	54	2242	335	2.55
1300	128	4502	2218	1.07
1600	250	7922	6820	1.59
1900	250	7922	6349	2.57
2100	432	12742	19491	1.06
2300	432	12742	19036	1.84

Table 6.3. Results of the performance analysis (circular duct) for the cubic enrichment $\{1, (x-x_0), (y-y_0), (z-z_0), (x-x_0)^2, (y-y_0)^2, (z-z_0)^2, (x-x_0)(y-y_0), (x-x_0)(z-z_0), (y-y_0)(z-z_0), (x-x_0)^3, (y-y_0)^3, (z-z_0)^3, (x-x_0)(y-y_0)(z-z_0), (x-x_0)^2(y-y_0), (x-x_0)^2(z-z_0), (x-x_0)(y-y_0)^2, (y-y_0)^2(z-z_0), (x-x_0)(z-z_0)^2, (y-y_0)(z-z_0)^2\}$

We also analyse both the assembly and solving time required for a frequency of 500 Hz. The value $T_{sloving}/T_{assembly}$ equals 0.64 for the constant enrichment and is around 0.005 for the other enrichments. This means that solving requirements are important for the constant enrichment, while for high order enrichments, the assembly of the matrices is huge compared to the time required by the solver. It is also important to note that the same mesh (for high order enrichments) is admissible over a large frequency range (i.e. 54 elements for the third order enrichment gives accurate results from 300 to 1000 Hz). We also know that the matrices of the system are frequency independant as long as we deal with polynomial enrichment functions. Then, for a multiple frequency analysis (usual in acoustics) the assembly (time consuming part) could be performed once while the solving (marginal compared to the assembly) needs to be performed for each frequency. It is not the same for the constant enrichment for which the solving time can not be neglected compared to the assembly.

6.1.2 Rectangular cross-section

We simulate a plane wave propagation in a duct for which the length is $L = 1m$ and the edges of the rectangular cross-section are $1m$ wide. The plane wave is prescribed with Neumann boundary conditions on the cross sections located at $z = 0$ and $z = L$.

A performance analysis (figure 6.3) is performed to compare the efficiency of the method. This is the reason why we plot the computational time with respect to the non-dimensional wavenumber (kD). The computational time corresponds to the time required to generate the mesh, compute the matrices of the system and solve the application with a given kD such that the accuracy (L^2 relative error) remains bounded: $\varepsilon_r \leq 5\%$. The mesh is chosen to have $2j$ elements along the axial direction and $j \times j$ within the cross-section. We observe, as it is shown for axisymmetric models, that it is more convenient to use high order enrichments. For the same amount of computational time, higher frequencies can be computed with higher enrichment order. We may also conclude that the computation for a given frequency requires less time for higher enrichment order. Computations require huge amount of time as soon as we exceed $kD = 20$ for the constant enrichment (degenerated linear FEM). In the case of higher order enrichment, this limit is moved to higher non-dimensional wavenumbers ($kD = 40$).

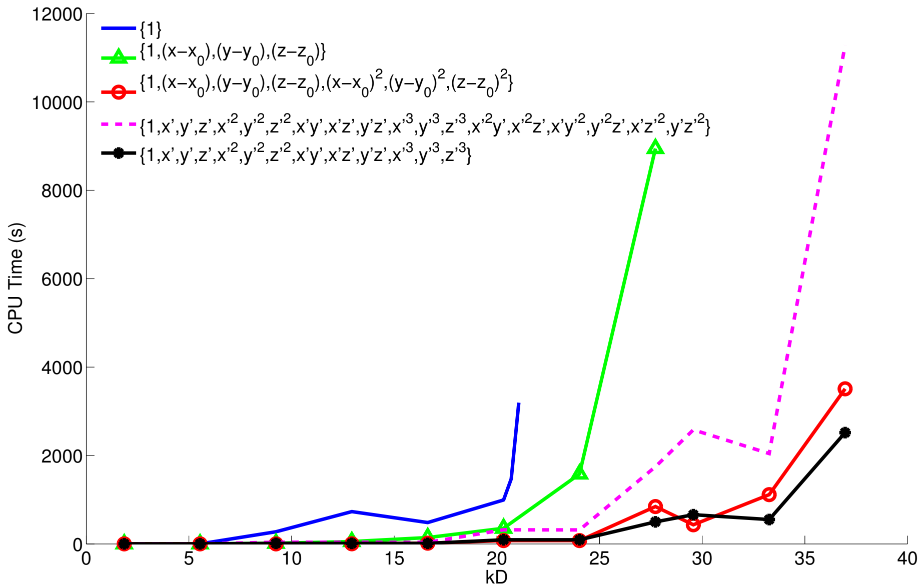

Fig. 6.3. Computational Time (s) versus the non-dimensional wavenumber (kD) with an accuracy under 5%, frequency varying from 100Hz to 2000Hz (1140Hz *for the constant enrichment:* $V_{jl} = \{1\}$), the characteristic length $D = 1m$ is one edge of the rectangular cross-section. Some simplifications have been made, terms of the legend such as $\{x', y', ...\}$ have to be read as $\{(x - x_0), (y - y_0), ...\}$)

As it has been done for the duct with the circular cross-section, tables 6.4, 6.5 and 6.6 give further of informations to figure 6.3. We see the huge increase of degrees of freedom with the frequency for the constant enrichment compared to the others. Note that the performed relative error with the third order enrichment is low compared to the prescribed 5% of accuracy.

6.1.3 Annular cross-section

We briefly illustrate the performances of the Mapped Infinite Partition of Unity Method for acoustic propagation in an annular duct ($r_i = 0.2m$ and $r_o = 0.5m$).

Frequency (Hz)	Elements	Dofs	CPU time (s)	ε_r (%)
100	2	12	1	4.24
300	432	637	2	4.84
500	31250	34476	276	4.77
700	54000	58621	732	4.97
900	43904	47937	484	4.85
1100	65536	70785	993	4.92
1120	78608	84525	1472	4.77
1140	118638	126400	3196	4.85

Table 6.4. Results of the performance analysis of the duct with a rectangular cross-section for the constant enrichment $\{1\}$

Frequency (Hz)	Elements	Dofs	CPU time (s)	ε_r (%)
100	2	84	1	0.02
300	2	84	1	1.65
500	16	315	2	2.33
700	16	315	2	3.78
900	54	784	15	2.70
1100	128	1575	75	1.64
1300	128	1575	75	3.47
1500	432	4459	844	2.33
1600	250	2772	432	4.87
1800	432	4459	1115	3.64
2000	686	6720	3510	4.59

Table 6.5. Results of the performance analysis of the duct with a rectangular cross-section for the second order enrichment $\left\{1, (x-x_0), (y-y_0), (z-z_0), (x-x_0)^2, (y-y_0)^2, (z-z_0)^2\right\}$

If we consider the propagation of a plane wave at 800 Hz. The mesh is generated with 5 elements along the axial direction and 5×5 within the cross-section. The constant enrichment leads to a L^2 relative error of $\varepsilon_r = 1.12\%$ while the second order one leads to $\varepsilon_r = 0.000497\%$.

In the case of the propagation at 800 Hz of the second radial mode of the first azimuthal order with a mesh of 8 elements along the axial direction and 8×8 within the cross-section. The constant enrichment leads to $\varepsilon_r = 25\%$ while the second order gives $\varepsilon_r = 0.52\%$.

Frequency (Hz)	Elements	Dofs	CPU time (s)	ε_r (%)
100	2	240	2	0.01
300	2	240	2	0.22
500	16	900	38	0.10
700	16	900	39	0.87
900	16	900	36	1.97
1100	54	2240	318	0.64
1300	54	2240	317	1.83
1500	128	4500	1746	1.18
1600	128	4500	2581	1.18
1800	128	4500	2043	2.64
2000	250	7920	11283	1.85

Table 6.6. Results of the performance analysis of the duct with a rectangular cross-section for the third order enrichment $\{1, (x-x_0), (y-y_0), (z-z_0), (x-x_0)^2, (y-y_0)^2, (z-z_0)^2, (x-x_0)(y-y_0), (x-x_0)(z-z_0), (y-y_0)(z-z_0), (x-x_0)^3, (y-y_0)^3, (z-z_0)^3, (x-x_0)(y-y_0)(z-z_0), (x-x_0)^2(y-y_0), (x-x_0)^2(z-z_0), (x-x_0)(y-y_0)^2, (y-y_0)^2(z-z_0), (x-x_0)(z-z_0)^2, (y-y_0)(z-z_0)^2\}$

We observe the same behaviour if for the same application we consider a uniform mean flow of $\mathbf{v}_0 = -100m/s\mathbf{1}_z$: constant enrichment and second order one leads to $\varepsilon_r = 98\%$ and $\varepsilon_r = 13\%$, respectively.

Note that this short analysis does not take into account the number of degrees of freedom nor the required CPU time. There is factor 5 between the number of degrees of freedom of constant and second order enrichment. We just illustrate that we can improve the accuracy without remeshing, just by increasing the order of the approximation.

6.1.4 Conclusion

These sections illustrate the performances of the Mapped Infinite Partition of Unity Method for the propagation in ducts (considered as cavities). Three different cross-sections and two boundary conditions are analysed. We may conclude that the use of high order enrichments is convenient to obtain good accuracy with low CPU time and to avoid remeshing.

6.2 Multipole radiation

We analyse the performances of the Mapped Infinite Partition of Unity Method for exterior three-dimensional applications. We simulate the propagation of a multipole by considering a quarter of sphere which vibrates (as it is done in the three-dimensional verification section 4.2).

We first plot the L^2 relative error (computed in the inner region) with respect to the number of degrees of freedom (figure 6.4) in order to compare the accuracy of the method. The vibrating (quarter of) sphere has a radius $r_1 = 1m$ and the interface Γ is located at $r_2 = 2m$. The inner region is meshed with $6\,(j \times j)$ elements on the sphere and $3j$ elements along the radial direction (j being a parameter of the convergence analysis). The number of infinite elements equals the number of elements on the vibrating sphere.

This analysis is performed with a constant frequency: $300Hz$ (corresponding to a non-dimensional wavenumber of $kR = 5.54$ with $R = 1m$ being the radius of the vibrating sphere). The prescribed velocity corresponds to the radiation of a multipole of order $N = 2$ with an azimuthal order equal to zero: $m = 0$. The radial order of the infinite element functions is chosen to be $m_0 = N + 1 = 3$ and $b_0 = 1$ which leads to linear circumferential functions.

Figure 6.4 illustrates the convergence rate of the Mapped Infinite Partition of Unity Method for three enrichments: constant, linear and second order. We observe that the convergence rate and the accuracy increase with the enrichment order.

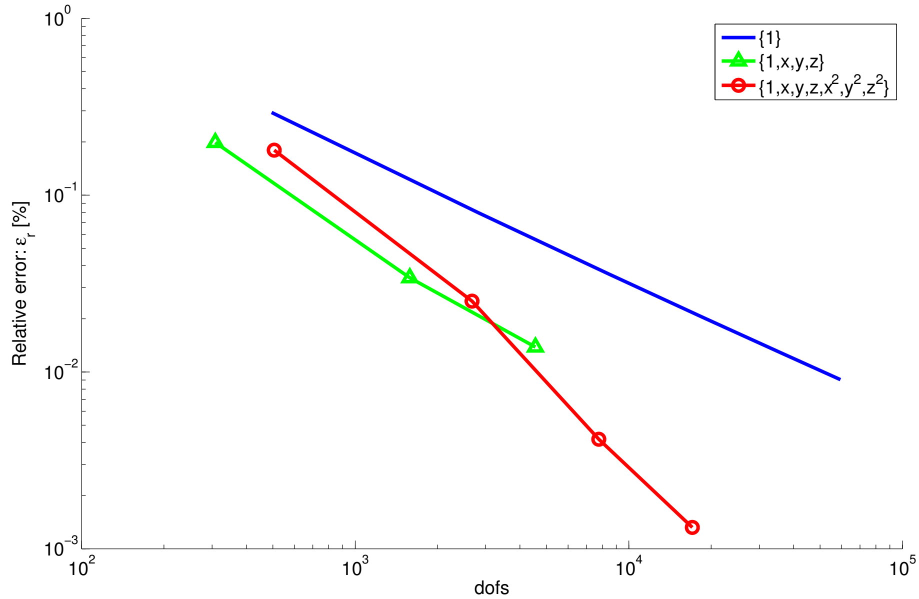

Fig. 6.4. Relative error ($\varepsilon_r = 1 means$ 100% *of error*) plotted with respect to the number of degrees of freedom (dofs): radiation at 300 Hz ($kR_d = 5.54$) of a multipole of order $N = 2$ and azimuthal order $m = 0$.

We also illustrate the efficiency of the method by comparing the CPU time required to solve the multipole radiation within an accuracy of less than $\varepsilon_r \leq 5\%$ (fig. 6.5). The radius of the vibrating sphere is $r_1 = 1m$ and that of the interface Γ: $r_2 = 2m$. The mesh is generated with $6\,(j \times j)$ elements on the vibrating sphere and $5j$ elements along the radial direction. We simulate the propagation of a multipole of order $N = 2$ and of azimuthal order $m = 0$. The range of frequencies analysed varies from 100 Hz to 1200 Hz (note that this analysis is limited to 800Hz for the constant enrichment). The radial order of the infinite element functions is chosen to be $m_0 = N + 1 = 3$ and $b_0 = 1$ which leads to linear circumferential functions.

Figure 6.5 illustrates that the CPU time required varies exponentially with the non-dimensional wavenumber. A small increase in the wavenumber (after $kR = 15$ for the constant enrichment) requires huge additional time to compute an accurate solution. We also notice that the CPU time required to compute the solution in the case of high enrichment order is high for low frequencies (low kR). This is due to the number of degrees of freedom per node and the integration scheme for high order polynomials. For instance, the third order enrichment leads to $4147s$ for 100Hz. However, the mesh is generated with the parameter $j = 2$ then only 168 elements and 24 infinite elements. But this low number of elements leads to high number of degrees of freedom (5346) and a lot of numerical integration points in the inner and outer regions[3]. Note that this discretization gives accurate results over a large frequency range (i.e. $f = 400$Hz, $kR = 7.39$ leads to an error of 3.54%).

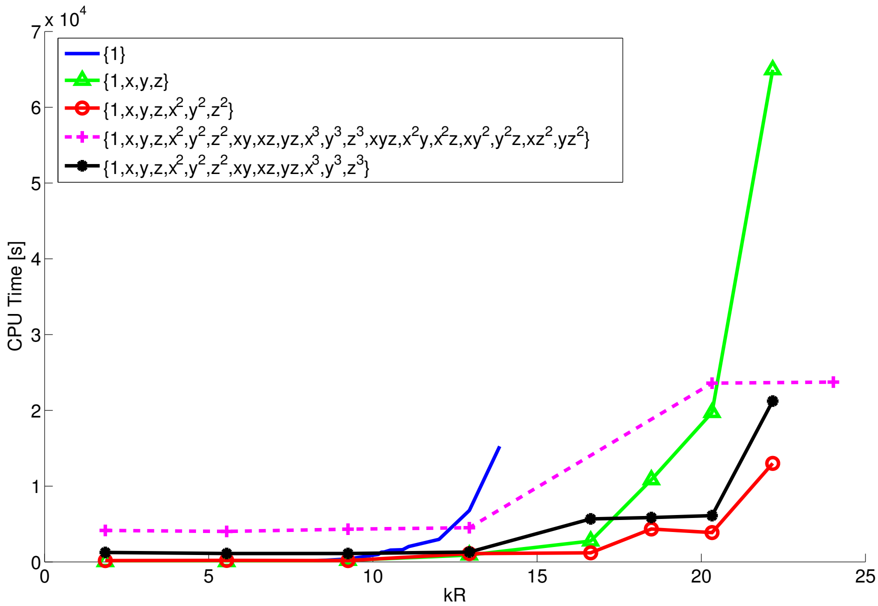

Fig. 6.5. Computational Time (s) versus the non-dimensional wavenumber (kR) with an accuracy under 5%, frequency varying from 100Hz to 1200Hz (to 800Hz for the constant enrichment), the characteristic length R is the radius of the vibrating sphere.

[3] For instance, the use of enrichment functions based on parent element coordinates (instead of global coordinates), would allow to compute the shape functions at the integration points once for all elements and then reduce the CPU time for the assembly of the matrices

We also decide to evaluate the influence of the parameter b_0. We consider the radiation at 150 Hz of a multipole of order $N = 7$ (then an infinite radial order of $m_0 = 8$) and azimuthal order $m = 0$. We use in the inner region the second order enrichment $\{1, x, y, z, x^2, y^2, z^2\}$. The radius of the vibrating sphere is $r_1 = 1m$ and the number of elements on this surface is $6\,(4 \times 4)$. We then compare the L^2 relative error in the inner region by choosing successively $b_0 = 0,\ 1\ \mathit{and}\ 2$. We consider the interface located at the radius $r_2 = 1.01m$ and one element along the radial direction. We obtained $\varepsilon_r = 7.28\%$ for $b_0 = 0$, $\varepsilon_r = 4.91\%$ for $b_0 = 1$ and $\varepsilon_r = 4.69\%$ for $b_0 = 2$. The accuracy is improved by increasing the interpolation in the circumferential direction.

We may conclude that it is convenient to use a high enrichment order to obtain accurate solution and to reach higher frequencies. Nevertheless a low number of elements with high order enrichments leads to high number of degrees of freedom, then requires a huge amount of CPU time even for low frequency. High order enrichments are then more convenient at high frequencies.

References

1. Ph. Bouillard, F. Ihlenburg, Error estimation and adaptivity for the finite element solution in acoustics: 2D and 3D applications, Comput. Methods Appl. Mech. Engrg. 176 (1999) 147-163.
2. F. Ihlenburg, I. Babuška, Dispersion analysis and error estimation of Galerkin finite element methods for the Helmholtz equation, Int. J. Numer. Methods Eng. 38 (1995) 3745-3774.
3. J.T. Oden, S. Prudhomme, L. Demkowicz, A posteriori error estimation for acoustic wave propagation problems, Arch. Comput. Meth. Engng. 12 (2005) 343-389.
4. F. Ihlenburg, I. Babuška, Finite element solution of the Helmholtz equation with high wave number part II : the h-p version of the FEM, SIAM J. Numer. Anal. 34 (1997) 315-358.
5. O.C. Zienkiewicz, Achievements and some unsolved problems of the finite element method, Int. J. Numer. Methods Eng. 47 (2000) 9-28.
6. L.L. Thompson, A review of finite element methods for time-harmonic acoustics, J. Acoust. Soc. Am. 119 (2006) 1315-1330.
7. J.M. Melenk, I. Babuška, The partition of unity finite element method: basic theory and applications, Comput. Methods Appl. Mech. Engrg. 139 (1996) 289-314.
8. I. Babuška, J.M. Melenk, The Partition of Unity Method, Int. J. Numer. Methods Eng. 40 (1997) 727-758.
9. O. Laghrouche, P. Bettess, R. J. Astley, Modeling of short wave diffraction problems using approximating systems of plane waves, Int. J. Numer. Methods Eng. 54 (2002) 1501-1533.
10. Th. Strouboulis, I. Babuška, R. Hidajat, The generalized finite element method for Helmholtz equation: Theory, computation, and open problems, Comput. Methods Appl. Mech. Engrg. 195 (2006) 4711-4731.
11. Th. Strouboulis, R. Hidajat, I. Babuška, The generalized finite element method for Helmholtz equation Part II: Effect of choice of handbook functions, error due to absorbing boundary conditions and its assessment, Comput. Methods Appl. Mech. Engrg. 197 (2008) 364-380.
12. Th. Strouboulis, K. Copps, I. Babuška, The generalized finite element method, Comput. Methods Appl. Mech. Engrg. 190 (2001) 4081-4193.
13. Th. Strouboulis, I. Babuška, K. Copps, The design and analysis of the generalized finite element method, Comput. Methods Appl. Mech. Engrg. 181 (2000) 43-69.
14. C. Farhat, I. Harari, L.P. Franca, The discontinuous enrichment method, Comput. Methods Appl. Mech. Engrg. 190 (2001) 6455-6479.
15. B. Pluymers, W. Desmet, D. Vandepitte, P. Sas, Application of an efficient wave-based prediction technique for the analysis of vibro-acoustic radiation problems, J. Comput. Appl. Math. 168 (2004) 353-364.
16. P. Gamallo, R.J. Astley, A comparison of two Trefftz-type methods: The ultraweak variational formulation and the least-squares method, for solving shortwave 2-D Helmholtz problems, Int. J. Numer. Methods Eng. 71 (2007) 406-432.
17. P. Gamallo, R.J. Astley, The partition of unity finite element method for short wave acoustic propagation on non-uniform potential flows, Int. J. Numer. Methods Eng. 65 (2006) 425-444.
18. T. Huttunen, P. Gamallo, R.J. Astley, Comparison of two wave element methods for the Helmholtz problem, Commun. Numer. Meth. Engng. Article in Press (2008) doi:10.1002/cnm1102.
19. T. Huttunen, P. Monk, J.P. Kaipio, Computational aspects of the ultra weak variational formulation, J. Comput. Phys. 182 (2002) 27-46.
20. T. Huttunen, J.P. Kaipio, P. Monk, An ultra weak method for acoustic fluid-solid interaction, J. Comput. Appl Math. 213 (2008) 166-185.

21. P. Monk, D.-Q. Wang, A least squares method for the Helmholtz equation, Comput. Methods Appl. Mech. Engrg. 175 (1999) 121-136.
22. R. Sevilla, S. Fernández-Méndez, A. Huerta, NURBS-enhanced finite element method (NEFEM), Int. J. Numer. Methods Eng. Early ViewW (2008) doi: 10.1002/nme.2311
23. E. Chadwick, P. Bettess, O. Laghrouche, Diffraction of short waves modeled using new mapped wave envelope finite and infinite elements, Int. J. Numer. Methods Eng. 45 (1999) 335-354.
24. E. De Bel, P. Villon, Ph. Bouillard, Forced vibrations in the medium frequency range solved by a partition of unity method with local information, Int. J. Numer. Methods Eng. 162 (2004) 1105-1126.
25. L. Hazard, Ph. Bouillard, Structural dynamics of viscoelastic sandwich plates by the partition of unity finite element method, Comput. Methods Appl. Mech. Engrg. 196 (2007) 4101-4116.
26. T.J.R. Hughes, J.A. Cotrell, Y. Bazilevs, Isogeometric analysis: CAD, finite elements, NURBS, exact geometry and mesh refinement, Comput. Methods Appl. Mech. Engrg. 194 (2005) 4135-4195.
27. B. Szabó, A. Düster, E. Rank, The p-version of the finite element method, in: E. Stein, R. de Borst, T.J.R. Hughes (Eds.), Fundamentals, Encyclopedia of Computational Mechanics, vol. 1, Wiley, New York, 2004 (Chapter 5).
28. R.J. Astley, P. Gamallo, Special short wave elements for flow acoustics, Comput. Methods Appl. Mech. Engrg. 194 (2005) 341-353.
29. R.J. Astley, P. Gamallo, The Partition of Unity Finite Element Method for Short Wave Acoustic Propagation on Non-uniform Potential Flows, Int. J. Numer. Methods Eng. 65 (2006) 425-444.
30. R.J. Astley, G.J. Macaulay, J.-P. Coyette, L. Cremers, Three-dimensional wave-envelope elements of variable order for acoustic radiation and scattering. Part I. Formulation in the frequency domain, J. Acoust. Soc. Am. 103 (1998) 49-63.
31. R.J. Astley, J.-P. Coyette, Conditioning of infinite element schemes for wave problems, Commun. Numer. Meth. Engng. 17 (2001) 31-41.
32. D. Dreyer, O. von Estorff, Improved conditioning of infinite elements for exterior acoustics, Int. J. Numer. Methods Eng. 58 (2003) 933-953.
33. J.J. Shirron, I. Babuška, A comparison of approximate boundary conditions and infinite element methods for exterior Helmholtz problems, Comput. Methods Appl. Mech. Engrg. 164 (1998) 121-139
34. D. Dreyer, Efficient infinite elements for exterior acoustics, PhD thesis, Shaker Verlag, Aachen, 2004.
35. W. Eversman, Mapped infinite wave envelope elements for acoustic radiation in a uniformly moving medium, J. Sound Vib. 224 (1999) 665-687.
36. S.J. Rienstra, W. Eversman, A numerical comparison between the multiple-scales and finite-element solution for sound propagation in lined flow ducts, J. Fluid Mech. 437 (2001) 367-384.
37. S.J. Rienstra, Sound transmission in slowly varying circular and annular lined ducts with flow, J. Fluid Mech. 380 (1999) 279-296.
38. S.J. Rienstra, The Webster equation revisited, 8th AIAA/CEAS Aeroacoustic conference (2002) AIAA 2002-2520.
39. M.K. Myers, On the acoustic boundary condition in the presence of flow, J. Sound Vib. 71 (1980) 429-434.
40. T. Mertens, Meshless modeling of acoustic radiation in infinite domains, Travail de spécialisation, Université Libre de Bruxelles (U.L.B.), 2005.
41. W. Eversman, The boundary condition at an impedance wall in a non-uniform duct with potential mean flow, J. Sound Vib. 246 (2001) 63-69.
42. B. Regan, J. Eaton, Modeling the influence of acoustic liner non-uniformities on duct modes, J. Sound Vib. 219 (1999) 859-879.
43. H.-S. Oh, J.G. Kim, W.-T. Hong, The Piecewise Polynomial Partition of Unity Functions for the Generalized Finite Element Methods, Comput. Methods Appl. Mech. Engrg. Accepted manuscript (2008), doi: 10.1016/j.cma.2008.02.035.
44. Free Field Technologies, Actran user's manual, http://fft.be.
45. University of Florida, Department of Computer and Information Science and Engineering, http://www.cise.ufl.edu/research/sparse/umfpack/
46. T.A. Davis, A column pre-ordering strategy for the unsymmetric-pattern multifrontal method, ACM Transactions on Mathematical Software 30 (2004) 165-195.
47. T.A. Davis, Algorithm 832: UMFPACK, an unsymmetric-pattern multifrontal method, ACM Transactions on Mathematical Software 30 (2004) 196-199.
48. T.A. Davis and I.S. Duff, A combined unifrontal/multifrontal method for unsymmetric sparse matrices, ACM Transactions on Mathematical Software 25 (1999) 1-19.

49. T.A. Davis and I.S. Duff, An unsymmetric-pattern multifrontal method for sparse LU factorization, SIAM Journal on Matrix Analysis and Applications 18 (1997) 140-158.
50. A. Hirschberg, S.W. Rienstra, An introduction to aeroacoustics, Eindhoven University of Technology (2004).
51. G. Warzée, Mécanique des solides et des fluides, Université Libre de Bruxelles (2005).
52. M.J. Crocker, Handbook of acoustics, Wiley-Interscience, New York (1998).
53. R. Sugimoto, P. Bettess, J. Trevelyan, A numerical integration scheme for special quadrilateral finite elements for the helmholtz equation, Commun. Numer. Meth. Engng. 19 (2003) 233-245.
54. G. Gabard, R.J. Astley, A computational mode-matching approach for sound propagation in three-dimensional ducts with flow, J. Sound Vib. Article in Press (2008) doi:10.1016/j.jsv.2008.02.015.
55. C. Farhat, I. Harari, U. Hetmaniuk, A discontinuous Galerkin method with Lagrange multipliers for the solution of Helmholtz problems in the mid-frequency regime, Comput. Methods Appl. Mech. Engrg. 192 (2003) 1389-1419.
56. C.L. Morfey, Acoustic energy in non-uniform flows, J. Sound Vib. 14 (1971) 159-170.
57. F. Magoules, I. Harari (editors), Special issue on Absorbing Boundary Conditions, Comput. Methods Appl. Mech. Engrg. 195 (2006) 3354-3902.
58. M. Fischer, U. Gauger, L. Gaul, A multipole Galerkin boundary element method for acoustics, Engineering Analysis with Boundary Elements 28 (2004) 155-162.
59. J.-P. Bérenger, Three-dimensional Perfectly Matched Layer for the absorption of electromagnetic waves, J. Comput. Phys. 127 (1996) 363-379.
60. C. Michler, L. Demkowicz, J. Kurtz, D. Pardo, Improving the performance of Perfectly Matched Layers by means of hp-adaptivity, Numerical Methods for Partial Differential Equations 23 (2007) 832-858.
61. A. Bayliss, E. Turkel, Radiation boundary conditions for wave-like equations, Comm. Pure Appl. Math. 33 (1980) 707-725.
62. B. Engquist, A. Majda, Radiation boundary conditions for acoustic and elastic wave calculations, Comm. Pure Appl. Math. 32 (1979) 313-357.
63. K. Feng, Finite element method and natural boundary reduction, Proceedings of the International Congress of Mathematicians, Warsaw (1983) 1439-1453.
64. D. Givoli, B. Neta, High-order non-reflecting boundary scheme for time-dependent waves, J. Comput. Phys. 186 (2003) 24-46.
65. T. Hagstrom, A. Mar-Or, D. Givoli, High-order local absorbing conditions for the wave equation: Extensions and improvements, J. Comput. Phys. 227 (2008) 3322-3357.
66. T. Hagstrom, T. Warburton, A new auxiliary variable formulation of high-order local radiation boundary conditions: corner compatibility conditions and extensions to first order systems, Wave Motion 39 (2004) 327-338.
67. A. Hirschberg, S.W. Rienstra, An introduction to aeroacoustics, Eindhoven university of technology (2004).
68. V. Lacroix, Ph. Bouillard, P. Villon, An iterative defect-correction type meshless method for acoustics, Int. J. Numer. Meth. Engng 57 (2003) 2131-2146.
69. T. Mertens, P. Gamallo, R. J. Astley, Ph. Bouillard, A mapped finite and infinite partition of unity method for convected acoustic radiation in axisymmetric domains, Comput. Methods Appl. Mech. Engrg. 197 (2008) 4273-4283.
70. G. Gabard, Discontinuous Galerkin methods with plane waves for time harmonic problems, J. Comput. Phys. 225 (2007) 1961-1984.
71. L. Hazard, Design of viscoelastic damping for vibration and noise control: modeling, experiments and optimisation, PhD thesis, Univesité Libre de Bruxelles (2007).
72. G. Gabard, R.J. Astley, M. Ben Tahar, Stability and accuracy of finite element methods for flow acoustics. I: general theory and application to one-dimensional propagation, Int. J. Numer. Meth. Eng. 63, (2005) 947-973.
73. G. Gabard, R.J. Astley, M. Ben Tahar, Stability and accuracy of finite element methods for flow acoustics. II: Two-dimensional effects, Int. J. Numer. Meth. Eng. 63 (2005) 974-987.
74. A. Goldstein, Steady state unfocused circular aperture beam patterns in non attenuating and attenuating fluids, J. Acoust. Soc. Am. 115 (2004) 99-110.
75. T. Douglas Mast, F. Yu, Simplified expansions for radiation from baffled circular piston, J. Acoust. Soc. Am. 118 (2005) 3457-3464.
76. T. Hasegawa, N. Inoue, K Matsuzawa, A new rigorous expansion for the velocity potential of a circular piston source, J. Acoust. Soc. Am. 74 (1983) 1044-1047.
77. R.J. Astley, A finite element, wave envelope formulation for acoustical radiation in moving flows, J. Sound Vib. 103 (1985) 471-485.
78. J.M. Tyler, T.G. Sofrin, Axial flow compressor noise studies, SAE Transactions 70 (1962) 309-332.

79. M.C. Duta, M.B. Giles, A three-dimensional hybrid finite element/spectral analysis of noise radiation from turbofan inlets, J. Sound Vib. 296 (2006) 623-642.
80. H.H. Brouwer, S.W. Rienstra, Aeroacoustics research in Europe: The CEAS-ASC report on 2007 highlights, J. Sound Vib. Article in Press (2008) doi:10.1016/j.jsv.2008.07.020.
81. http://en.wikipedia.org/wiki/Aircraft_noise, 4th September 2008.
82. Y. Park, S. Kim, S. Lee, C. Cheong, Numerical investigation on radiation characteristics of discrete-frequency noise from scarf and scoop aero-intakes, Appl. Acoust. Article in press (2008) doi:10.1016/j.apacoust.2007.09.005.
83. General Electric Company, http://www.ge.com, http://www.turbokart.com/about_ge90.htm, 4th September 2008.
84. R.J. Astley, J.A. Hamilton, Modeling tone propagation from turbofan inlets - The effect of extended lip liner, AIAA paper 2002-2449 (2002).
85. V. Decouvreur, Updating acoustic models: a constitutive relation error approach, PhD thesis, Université Libre de Bruxelles (2008).
86. P.A. Nelson, O. Kirkeby, T. Takeuchi, and H. Hamada, Sound fields for the production of virtual acoustic images, Letters to the editor, J. Sound Vib. 204 (1999) 386-396.
87. Y. Reymen, W. De Roeck , G. Rubio, M. Bealmans, W. Desmet, A 3D Discontinuous Galerkin Method for aeroacoustic propagation, Proceedings of the 12th International Congress on Sound and Vibration 2005.
88. G. Gabard, Exact integration of polynomial-exponential products with an application to wave based numerical methods, Commun. Numer. Meth. Engng (2008) doi: 10.1002/cnm.1123.
89. New York University, http://math.nyu.edu/faculty/greengar/shortcourse_fmm.pdf, 1st december 2008.